Neurobiology of Disease 124 (2019) 322–334

Contents lists available at ScienceDirect

Neurobiology of Disease

journal homepage: www.elsevier.com/locate/ynbdi

Induced neural progenitor cells abundantly secrete extracellular vesicles and promote the proliferation of neural progenitors via extracellular signal–regulated kinase pathways

Yizhao Ma[a,1], Kaizhe Wang[a,1], Jiabin Pan[a], Zhaohuan Fan[a], Changhai Tian[a,c], Xiaobei Deng[a], Kangmu Ma[a,c], Xiaohuan Xia[a,*], Yunlong Huang[a,c,*], Jialin C. Zheng[a,b,c,d,*]

[a] Center for Translational Neurodegeneration and Regenerative Therapy, Shanghai Tenth People's Hospital affiliated to Tongji University School of Medicine, Shanghai 200072, China
[b] Collaborative Innovation Center for Brain Science, Tongji University, Shanghai 200092, China
[c] Departments of Pharmacology and Experimental Neuroscience, University of Nebraska Medical Center, Omaha, NE 68198-5930, USA
[d] Department of Pathology and Microbiology, University of Nebraska Medical Center, Omaha, NE 68198-5930, USA

ARTICLE INFO

Keywords:
Cellular reprogramming
Neural progenitor cells
Extracellular vesicles
Proliferation
Growth factors
ERK pathways

ABSTRACT

Neural stem/progenitor cells (NPCs) are known to have potent therapeutic effects in neurological disorders through the secretion of extracellular vesicles (EVs). Despite the therapeutic potentials, the numbers of NPCs are limited in the brain, curbing the further use of EVs in the disease treatment. To overcome the limitation of NPC numbers, we used a three transcription factor (Brn2, Sox2, and Foxg1) somatic reprogramming approach to generate induced NPCs (iNPCs) from mouse fibroblasts and astrocytes. The resulting iNPCs released significantly higher numbers of EVs compared with wild-type NPCs (WT-NPCs). Furthermore, iNPCs-derived EVs (iNPC-EVs) promoted NPC function by increasing the proliferative potentials of WT-NPCs. Characterizations of EV contents through proteomics analysis revealed that iNPC-EVs contained higher levels of growth factor-associated proteins that were predicted to activate the down-stream extracellular signal-regulated kinase (ERK) pathways. As expected, the proliferative effects of iNPC-derived EVs on WT-NPCs can be blocked by an ERK pathway inhibitor. Our data suggest potent therapeutic effects of iNPC-derived EVs through the promotion of NPC proliferation, release of growth factors, and activation of ERK pathways. These studies will help develop highly efficient cell-free therapeutic strategies for the treatment of neurological diseases.

1. Introduction

Due to the limited number of endogenous neural stem/progenitor cells (NPCs) in adults, transplantation with exogenous NPCs has been proposed as a promising therapeutic strategy in treating neurodegenerative diseases (Ager et al., 2015; Goldberg et al., 2017; Zhang et al., 2014) and traumatic brain injury (Hou et al., 2017; Tang et al., 2014). Transplanted NPCs were originally shown to replace damaged neuronal and glial cells. However, recent studies revealed that transplanted NPCs might achieve therapeutic effects through modulation of microenvironment for the endogenous NPCs (Lee et al., 2013; Yarygin et al., 2009). Extracellular vesicles (EVs), which are released from virtually all cell types in the brain, are a key component of the central nervous system microenvironment (Zappulli et al., 2016). EVs are heterogeneous nanoscale membranous vesicles that include exosomes (EXOs), microvesicles (MVs), and apoptotic bodies. EV contain proteins such as enzymes, cytokines, nucleic acids, and other bioactive molecules (Hessvik and Llorente, 2018; Raposo and Stoorvogel, 2013; Tetta et al., 2013). EVs are known to modulate neuronal functions in both nervous system development and adults (Feliciano et al., 2014; Schiera et al., 2015). In addition, EVs may also regulate other components of neurogenic niches and help maintain the balance between proliferation and differentiation of NPCs (Batiz et al., 2015). Mesenchymal stem cell-derived EVs (MSC-EVs) are able to promote long-term neuroprotection, post-stroke regeneration, and other functions of NPCs (Doeppner et al., 2015; Otero-Ortega et al., 2017). Compared to MSC-EVs, human neural stem cell-derived EVs (hNSCs-EVs) may be more effective in improving cellular, tissue, and functional outcomes in a murine thromboembolic

* Corresponding authors at: Center for Translational Neurodegeneration and Regenerative Therapy, Shanghai Tenth People's Hospital affiliated to Tongji University School of Medicine, Shanghai 200072, China.
E-mail addresses: xiaohuan_xia1@163.com (X. Xia), yhuan1@unmc.edu (Y. Huang), jialinzheng@tongji.edu.cn (J.C. Zheng).
[1] These authors contributed equally to this work.

https://doi.org/10.1016/j.nbd.2018.12.003
Received 8 May 2018; Received in revised form 16 November 2018; Accepted 3 December 2018
Available online 04 December 2018
0969-9961/

stroke model (Webb et al., 2017). Therefore, administration of EVs may be able to achieve similar favorable therapeutic outcome while having a lower risk of adverse effects compared with direct cell transplantation (Bobis-Wozowicz et al., 2015).

EVs assert effects on target cells through active molecules in their cargoes. For example, neuron-derived EVs contain synaptic plasticity-associated microtubule-associated protein 1B (MAP1B) and miRNAs, which participate in the activity-dependent synaptic plasticity, dendritic arborization, and formation of long-term memory (Goldie et al., 2014). NPCs-derived EVs contain asparaginase-like protein 1 (Asrgl1) that functions as an independent metabolic unit to regulate critical nutrients in the microenvironment (Iraci et al., 2017). In addition, NPC-derived EVs are also able to transfer mRNAs that are of regenerative potentials and help maintain the essential functions of NPCs (Yoshimura et al., 2018). Therefore, NPC-derived EVs have great therapeutic potentials in regenerative medicine. Understanding the functional impact of EVs and the EV contents is critical to the further use of NPCs-derived EVs in the disease treatment.

The development of cellular reprogramming technology has enabled the generation of induced NPCs (iNPCs) that provide adequate amounts of EVs for therapeutic purposes (Lai et al., 2015; Lujan et al., 2012; Shahbazi et al., 2016). In the current studies, we used iNPCs-derived EVs and found that these EVs promoted significantly higher levels of proliferative potentials of wild type (WT)-NPCs, compared with EVs derived from wild type NPCs (WT-EVs). We further analyzed the contents of the EVs and identified a specific increase of growth factors compared with those from WT-EVs. Furthermore, we determined that iNPC-EVs regulate the proliferation of WT-NPCs through activating the extracellular signal–regulated kinase pathways. These results suggest potent effects of iNPC-EVs on NPC functions, which can be harnessed to design novel cell-free therapeutic strategies for neurological disorders.

2. Materials and methods

2.1. Animals and reagents

C57BL/6 J and Nestin-EGFP mice were housed and maintained in the Comparative Medicine Facility of the Tongji University School of Medicine (Shanghai, China). All procedures were conducted in accordance with the protocols approved by the Institutional Animal Care and Use Committee at the Tongji University School of Medicine.

U0126(#S1102) was obtained from Selleck chemical. PKH26 (Sigma, #PKH26GL) was obtained from Sigma-Aldrich. Fluorescein Phalloidin (# F432) was obtained from Life technologies.

2.2. Mouse fibroblast isolation and enrichment

Mouse fibroblasts were derived from Nestin-EGFP transgenic mice embryos at 13.5–14.5 d post coitum as previously described (Tian et al., 2012). All internal organs, head, and spinal cord were removed. The remaining skin tissues were washed twice with PBS, and dissociated with 0.25% trypsin-EDTA solution. Mouse fibroblasts were cultured in DMEM supplemented with 10% FBS, 1% non-essential amino acid (non-AA), 100 U/ml penicillin, 100 μg/ml streptomycin at 37 °C in a 5% CO_2 humidified atmosphere.

2.3. Mouse astrocyte isolation and enrichment

Astrocytes were isolated from cortices at postnatal day 7 as previously described (Wang et al., 2017). Briefly, cortices from Nestin-EGFP transgenic mice were dissected and mechanically dissociated to remove the membranes and large blood vessels. After washed twice with HBSS, cortices were digested at 37 °C for 20 min by Trypsin-EDTA (Thermo Scientific). Digestion was stopped by FBS (Thermo Scientific). After trituration, cells were plated on T75 flask in DMEM/F12 with 10% FBS, 100 U/ml penicillin, 100 μg/ml streptomycin at 37 °C in a 5% CO_2 humidified atmosphere. The culture medium was replaced every three days. After three passages, astrocytes were harvested by trypsinization.

2.4. Mouse NPCs isolation and enrichment

Mouse cortical NPCs were isolated from mouse fetal brain tissue, as previously described (Chen et al., 2015). Briefly, NPCs were cultured in substrate-free tissue culture flasks for the formation of neurospheres in NPC proliferation medium, containing NeuroCult® NSC Basal Medium (Stem Cell Technologies), NeuroCult® NSC Proliferation Supplements (Stem Cell Technologies), 20 ng/ml FGF2 (BioWalkersville), 20 ng/ml EGF (BioWalkersville) and 2 μg/ml heparin (Sigma), N2 supplement, 2 mM L-glutamine, 100 U/ml penicillin, 100 μg/ml streptomycin. Primary neurospheres were collected, dissociated, and re-suspended into single cells for a second round of neurosphere formation. Enriched NPCs were harvested after three rounds of neurosphere formation.

2.5. Retroviral preparation

Plasmid encoding mouse Sox2 was purchased from Addgene. Mouse FoxG1 (restriction enzymes: *Bam*HI and *Xho*I), Brn2 (restriction enzymes: BamHI and XhoI) were amplified from mouse NPCs cDNA library. Each gene was individually cloned into pMXs-retroviral vectors (Cell Biolabs). For the preparation of retroviruses, Plat-E cells were seeded at 3.6×10^6 cells per 100-mm dish. 24 h after plating, pMXs-based retroviral vectors encoding Sox2, Brn2, FoxG1 and empty vector control were introduced into Plat-E cells using Lipofectamine™ LTX transfection reagent (Thermo Scientific) according to the protocol from the manufacturer. The medium was replaced with DMEM/F12 containing 10% FBS 24 h after transfection. At 48 h and 72 h post-transfection, virus-containing supernatants were collected and filtered through a 0.45-μm cellulose acetate filter.

2.6. Reprogramming of mouse astrocytes and fibroblasts

Fibroblasts and astrocytes were transduced with retroviruses in polybrene-containing (10 μg/ml) supernatants overnight. The second round of infection was carried out 3 days post-transfection. Infected astrocytes were changed to NPC proliferation medium contain mouse NeuroCult Basal Medium (Stem Cell Technologies) supplemented with 10% NeuroCult Proliferation Supplement, epidermal growth factor (EGF, 10 ng/ml, Sigma Aldrich) and basic fibroblast growth factor (FGF2, 20 ng/ml, Sigma Aldrich) 1 day after the second infection. NPC proliferation medium was changed every two days. 30 days after retroviral transduction, bulged colonies were manually picked, dissociated and re-suspended into single cells in Petri dishes. After the formation of primary neurospheres after culturing for 4–6 days, neurospheres were collected, dissociated and re-plated into Poly-D-Lysine/Fibronectin coated 6 well plates. Cells were collected at 80% confluency and re-suspended into single cells for a second round neurosphere formation. After 3 rounds of neurosphere formation, cells were collected for the validation of reprogramming.

2.7. Differentiation of NPCs

The differentiation of NPCs and iNPCs was as previously described (Tian et al., 2015). Briefly, 5000 NPCs were planted on Poly-L-Ornithine/laminin-coated coverslips in 24-well plate with DMEM/F12 supplemented with 1 × N2, 1 × B27, 1.0 mM Glutamax, 0.11 mM β-mercaptoethanol, 1.0 mM dibutyrylcAMP (Sigma), 0.2 mM ascorbic acid (Sigma), 10 ng/ml brain-derived neurotrophic factor (BDNF) (Peprotech), and 10 ng/ml glial cell line-derived neurotrophic factor (GDNF) (Peprotech) for 4 weeks. The medium was changed every 3–4 days.

2.8. Isolation of EVs

EVs were isolated from the serum-free culture of NPCs as previously described (Wu et al., 2018). Briefly, 6×10^6 NPC/iNPC were planted on poly-L-Ornithine/laminin-coated 10 cm dish and cultured in NPC proliferation medium for 12 h. The supernatants were first centrifuged at 300 ×*g* for 10 min to remove free cells, at 3000 ×g for 20 min to remove cellular debris, and then 10,000 ×g for 30 min to remove intracellular organelles. EVs were collected by ultracentrifugation at 100,000 ×*g* for 2 h. All centrifugation steps were performed at 4 °C.

2.9. Dynamic light scattering

Isolate EVs were re-suspended in 150 μl PBS, diluted at 1:100 in PBS. 8 μl samples were loaded into a microcuvette (ZEN0118, Malvern Instruments, UK) for measurement. Three determinations per sample were taken at 25 °C using Nano ZS90 (Malvern Instruments, UK) for each independent experiment. The size of EVs was measured by the fluctuations of scattered light intensity at a fixed angle using 633 nm wavelength laser. Data acquisition and analysis were performed using Malvern Zetasizer Software (Malvern Instruments, v7.03). The average particle diameter was calculated by the peak of intensity fitting to the particle distribution.

2.10. Nanoparticle tracking analysis (NTA)

The size and number of extracellular vesicles were carried out as previously described (Wu et al., 2018). Briefly, 8×10^6 WT-NPCs, FiNPCs, AiNPCs were planted on poly-L-Ornithine/laminin-coated 10-cm dish and cultured with 10 ml NPC proliferation medium, respectively. The culture supernatants were collected at 12 h, isolated EVs were resuspended in 150 μl PBS and diluted at 1:100 in PBS. 1 ml solution was used for NanoSight analysis. NTA was assessed on NanoSight NS300 system (Malvern Instruments, UK) with a sCMOS camera. The conditions of the measurements were set at 25 °C, 1 cP viscosity, 25 s per capture frame and 60 s measurement time. Three individual measurements were applied for the measurement of EVS sizes and concentration.

2.11. Scanning electron microscopy (SEM)

NPCs were grown on a glass coverslip, fixed with 2.5% glutaraldehyde, and washed three times with PBS. The cells were then dehydrated in a series of increasing ethanol concentrations and transferred for critical drying. After coating with platinum/palladium using a sputter coater, the sample was imaged with a scanning electron microscope (S-3400, Hitachi).

2.12. Transmission electron microscopy (TEM)

TEM of EVs: Purified EVs were negatively stained and then spread on the copper grids. The droplets of EVs were removed with filter paper and air-dried at room temperature.

TEM of NPCs: Collected NPCs pellet was fixed using 2.5% glutaraldehyde overnight at 4 °C and then washed twice with PBS. NPCs were fixed using 1% osmic acid for 1.5 h at room temperature. Followed by washing twice with PBS, NPCs were dehydrated in alcohol, embedded in epoxy resin, ultrasectioned, transferred to 300-mesh Formvar coated nickel grids (Electron Microscopy Sciences) and stained using 2% uranyl acetate and lead citrate.

Images were obtained using transmission electron microscopy (JEM-1230, JEOL Ltd.).

2.13. Western blot

EVs or cells were lysed in RIPA lysis and extraction buffer (Thermo Scientific). Protein concentration was determined using the BCA (bicinchoninic acid) Protein Assay Kit (Pierce). After electrophoretic transfer to polyvinyldifluoridene (PVDF) membranes (Millipore), proteins were treated with purified primary antibodies for Akt (1:1000; Cell Signaling Technologies), phospho-Akt (Ser473) (1:1000; Cell Signaling Technologies), MEK1/2 (1:1000; Cell Signaling Technologies), phospho-MEK1/2 (1:1000; Cell Signaling Technologies), ERK1/2(1:1000; Cell Signaling Technologies), phospho-ERK1/2(1:1000; Cell Signaling Technologies), β-actin (1:5000; Sigma Aldrich), flotillin-1 (1:1000;BD biosciences), flotillin-2 (1:5000;BD Biosciences), and HSP70 (1:1000; Cell Signaling Technologies) overnight at 4 °C. The density of the immunoblots was determined by image lab software and analyzed using Image J program.

2.14. Immunocytochemistry

The cultured cells were plated on coverslips and fixed in 4% formaldehyde for 20 min at room temperature and then washed with PBS for three times. The fixed cells were permeabilized with 0.2% Triton X-100 in PBS for 10 min, then blocked with 2% BSA in PBS for 1 h at room temperature. Subsequently, they were incubated overnight at 4 °C with primary antibodies including rabbit anti-Sox2 (1:1000; Cell Signaling Technologies), rabbit anti-MAP2 (1:1000; Millipore), rabbit anti-GABA (1:5000; Sigma), rabbit anti-VGLUT1/2 (1:100; synaptic systems), chicken anti-nestin (1:5000; Novus), mouse anti-βIII-Tubulin (Tuj1) (1:500; Sigma). Coverslips were washed and incubated for 1 h at room temperature with secondary antibodies including anti-rabbit IgG (coupled with Alexa Fluor 568, Life Technologies), anti-rabbit IgG (coupled with Alexa Fluor 488, Life Technologies) and anti-chicken IgG (coupled with Alexa Fluor 488, Life Technologies), anti-mouse IgG (coupled with Alexa Fluor 488, Life Technologies). Nuclear DNA was stained with DAPI. Then the coverslips were mounted on glass slides with mounting buffer (Sigma-Aldrich). Immunostaining was examined by a Zeiss 710 confocal laser scanning microscope.

2.15. EdU incorporation assay

DNA synthesis was performed by a Click-iT® EdU Imaging Kits (Thermo Scientific, #C10338) according to the manufacturer's instructions. 2.5×10^5 WT-NPCs were treated with 15 μg/ml EVs on 35 mm Coverglass-Bottom Dish (Cellvis, #161115) for 24 h, then changed NPC proliferation medium without EVs and cultured for another 24 h, EdU was added 2 h prior to fixation. Then the cells were fixed with 4% cold formaldehyde for 30 min at room temperature. After permeabilization with 1% Triton X-100, the cells were reacted with Click-iT® reaction cocktails (Thermo Scientific) for 30 min. Subsequently, the DNA contents of the cells were stained with DAPI. Images were taken using Zeiss AX10 fluorescence microscope and AxioVision Rel. 4.8 software. Image pro plus 6.0 was used for cell counting and EdU-labeled cells were normalized to the total number of DAPI-stained cells for statistical analysis.

2.16. Cell proliferation assay

Briefly, 15 μg/ml EVs were co-cultured with 5000 cells/well WT-NPCs on 96-well plates for 24 h, then changed with NPC proliferation medium without EVs and cultured for 48 h. Cell viability was measured by MTS (Promega, #G3582) and CCK-8 (Yeasen, #40203ES80) assays. Experiments were handled according to the manufacturer's instructions. Absorbance was measured at 570 nm and 450 nm and analyzed using SpectraMax M5 microplate readers (Molecular Devices).

2.17. Sample preparation and LC-MS/MS analysis

EVs or cells were lysed in RIPA lysis and extraction buffer (Thermo Scientific). The remaining debris was removed by centrifugation at

12,000 *g* at 4 °C for 10 min. The supernatant was collected and the protein concentration was determined with BCA kit (Thermo Scientific) according to the manufacturer's instructions. For trypsin digestion, the protein solution was reduced with 5 mM dithiothreitol for 30 min at 56 °C and alkylated with 11 mM iodoacetamide for 15 min at room temperature in darkness. The protein sample was then diluted by adding 100 mM TEAB to urea concentration < 2 M. Finally, trypsin was added at 1:50 trypsin-to-protein mass ratio for the first digestion overnight and 1:100 trypsin-to-protein mass ratio for a second digestion for 4 h. The tryptic peptides were dissolved in 0.1% formic acid (solvent A), directly loaded onto a home-made reversed-phase analytical column (15-cm length, 75 μm i.d.). The gradient was comprised of an increase from 6% to 23% solvent B (0.1% formic acid in 98% acetonitrile) over 26 min, 23% to 35% in 8 min and climbing to 80% in 3 min then holding at 80% for the last 3 min, all at a constant flow rate of 400 nL/min on an EASY-nLC 1000 UPLC system. The peptides were subjected to NSI source followed by tandem mass spectrometry (MS/MS) in Q ExactiveTM Plus (Thermo Scientific) coupled online to the UPLC. The electrospray voltage applied was 2.0 kV. The *m/z* scan range was 350 to 1800 for full scan, and intact peptides were detected in the Orbitrap at a resolution of 70,000. Peptides were then selected for MS/MS using NCE setting as 28 and the fragments were detected in the Orbitrap at a resolution of 17,500. A data dependent procedure that alternated between one MS scan followed by 20 MS/MS scans with 15.0 s dynamic exclusion. Automatic gain control (AGC) was set at 5E4. Fixed first mass was set as 100 m/z.

2.18. Protein identification and bioinformatics analysis

Tandem mass spectra were searched against UniProt database concatenated with reverse decoy database. Trypsin/P was specified as cleavage enzyme allowing up to 2 missing cleavages. The mass tolerance for precursor ions was set as 20 ppm in First search and 5 ppm in Main search, and the mass tolerance for fragment ions was set as 0.02 Da. Carbamidomethyl on Cys was specified as fixed modification and oxidation on Met was specified as variable modifications. FDR was adjusted to < 1% and minimum score for peptides was set > 40. After normalization, target features showing > 1.5-fold intensity differences were selected and denoted as differentially expressed proteins. For the identification of enriched protein domains, InterPro database was used and a two-tailed Fisher's exact test was employed to verify the enrichment of the differentially expressed protein against all identified proteins. Protein domains with a *p*-value < .05 were considered significant.

2.19. Statistical analyses

All results are the means of at least three independent experiments ± SD. Data were evaluated statistically by the analysis of variance (ANOVA), followed by Tukey's test for multiple comparisons. The Two-tailed Student's t test was used to compare two groups. Significance was considered when $p < .05$.

3. Results

3.1. iNPCs released more EVs than WT-NPCs

To characterize EVs derived from iNPCs, we first generated fibroblasts- and astrocytes-derived iNPCs (FiNPCs & AiNPCs) by ectopic expression of transcription factors Sox2, Brn2 and Foxg1 (Fig. S1A). The reprogramming was performed in the primary fibroblast and astrocyte cultures isolated from Nestin-EGFP mice following published protocols from our laboratory and others (Corti et al., 2012; Lujan et al., 2012; Ma et al., 2018; Tian et al., 2012). The immunocytochemical analysis demonstrated that both FiNPCs and AiNPCs expressed NPC markers SOX2 and Nestin (Fig. S1B) in proliferation medium, markers MAP2, vesicular transporter proteins for glutamate (VGLUT), and γ-aminobutyric acid (GABA) in differentiation medium (Fig. S1C), suggesting the NPC phenotype of the two iNPC lines. Interestingly, both iNPC lines had a higher proportion of proliferating cells in NPC proliferation medium, as determined by EdU staining, compared to WT-NPCs and NPCs isolated from Nestin-EGFP mice (Nestin-EGFP-NPCs) (Fig. S2A-F). The number of cells increased significantly in iNPCs groups at 24 h but not at 12 h, compared with those of WT-NPCs and Nestin-EGFP-NPCs, as determined by the quantification of DAPI-positive cells and CCK-8 assay (Fig. S2B, E, G-I). Therefore, this time point study suggests that the iNPCs have a higher proliferative capacities compared to those of WT-NPCs and Nestin-EGFP-NPCs. Since WT-NPCs and Nestin-EGFP-NPCs exhibited similar capacities in cell viability and proliferation, we used WT-NPCs as controls in the subsequent studies.

The proliferation of NPCs could be regulated by cell intrinsic and extrinsic factors (Huang et al., 2018; Wang et al., 2014). Our recent findings suggested that CNS cells could convey inter-cellular signaling through EVs secretion (Wang et al., 2017; Wu et al., 2015). To characterize the EVs, we used scanning electron microscopy (SEM) and found that EV-like polarized membranous structures were being released from the plasma membrane. Surprisingly, we found that these EV-like structures were quite abundant on the plasma membrane of FiNPCs and AiNPCs (Fig. 1A). In comparison, EV-like structures were less frequent on the plasma membrane of WT-NPC. The EV-like structures can be further visualized under transmission electron microscopy (TEM). The TEM data revealed individual EV-like structures with a circular shape that were being released from plasma membrane of the three types of NPCs (Fig. 1B). The SEM and TEM data of EVs were qualitative. To more definitively quantify EVs derived from the three types of NPCs, we isolated EVs from the serum-free culture through differential centrifugations to remove cell bodies, debris, and other EV contaminants. The resuspended EVs showed distinct cup-shaped EV morphology under negative staining in TEM, confirming that those vesicles released from the iNPCs/NPCs were indeed EVs (Fig. 1C). Next, we used the dynamic light scattering (DLS) and Nanoparticle tracking (NTA) analyses to more quantitatively measure EV size and concentration. Both DLS and NTA analyses demonstrated similar peaks for EVs released from FiNPCs (F-EVs), AiNPCs (A-EVs), and WT-NPCs (WT-EVs), suggesting there was no significant difference in size distributions of different types of EVs (Fig. 2A-C). Notably, DLS analysis revealed EVs two-fold larger in size compared to NTA analysis. This difference could be largely due to the physiological feature of DLS that favors the detection of larger particles over small particles.

To test whether more EVs are released from iNPCs than from WT-NPCs, we cultured the same number of each type of cells and collected EVs released from cells after 12 h, a time point when no significant difference in cell numbers was observed among all treatment groups (Fig. S2). NTA analysis showed significantly higher concentrations of EVs in F-EVs and A-EVs groups, compared with those from WT-EVs controls (Fig. 2C, D). We also observed no significant difference in the concentration of EVs released by either WT-NPCs or Nestin-EGFP-NPCs, suggesting that the higher capacity of EVs generation in iNPCs was not due to the transgene modification (Fig. S3). To validate the increased release of EVs in iNPCs, proteins were isolated from different types of EVs and then subjected to Western Blot for EVs specific markers, including Flotillin-1, Flotillin-2, and HSP70 (Fig. 2E). Consistent with NTA data, significantly higher levels of Flotillin-1, Flotillin-2, HSP70 were found in F-EVs and A-EVs groups, compared with those in WT-EVs group (Fig. 2F). Together, our data suggested that both FiNPCs and AiNPCs produced and released significantly higher levels of EVs, compared with WT-NPCs.

3.2. iNPC-derived EVs promote the proliferation of WT-NPCs

Because the strong association between high levels of EVs and the high proliferation rates, we hypothesized that iNPCs-mediated EVs

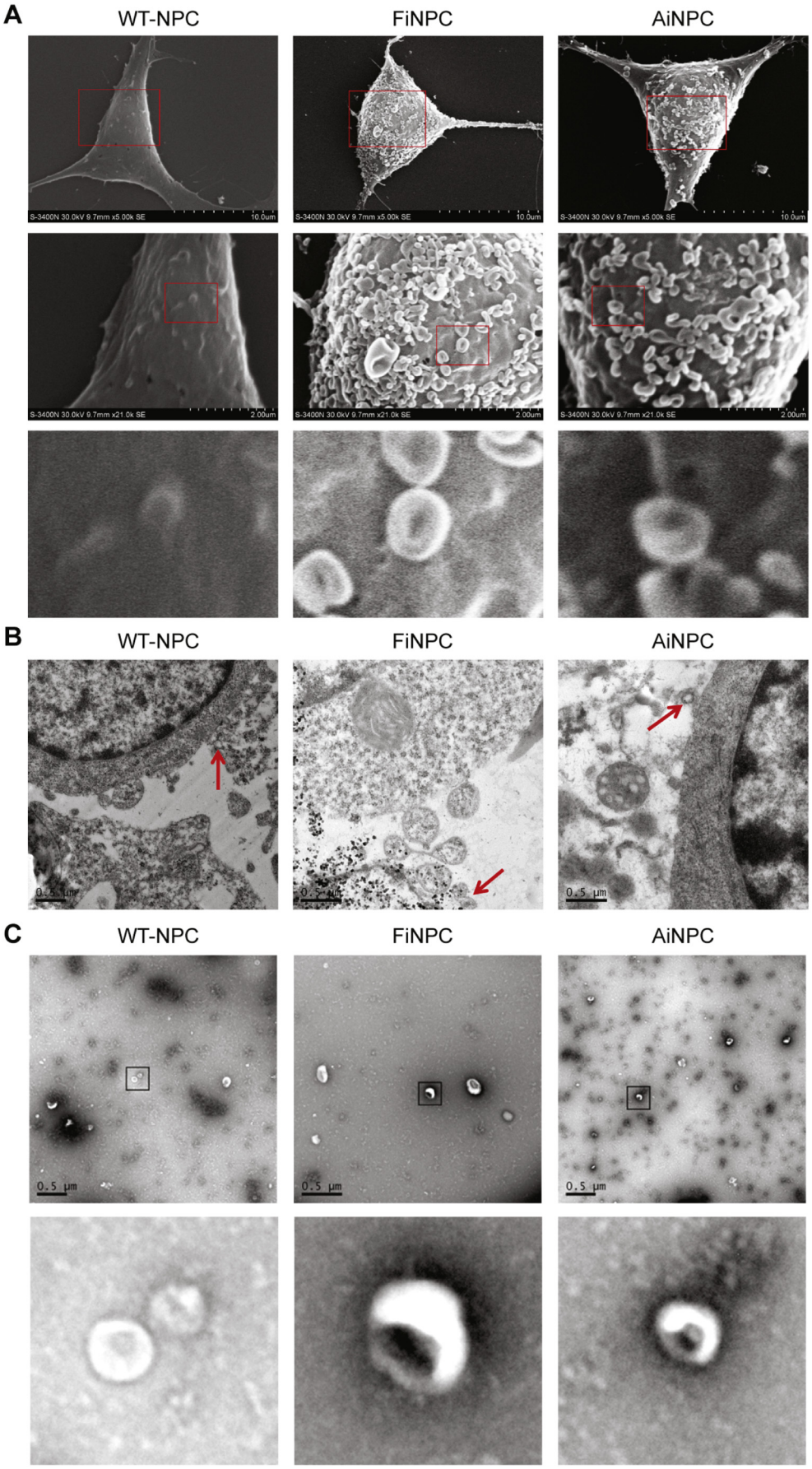

Fig. 1. Characterization of EVs released from WT-NPCs, FiNPCs, and AiNPCs. (A) Scanning electron microscope (SEM) image showing EVs adhered to cell's surface. The red boxes in the first raw were magnified in the second raw. The red boxes in the second raw were magnified in the third raw. (B) Transmission electron microscopy (TEM) shows the generation of EVs (red arrows). (C) EVs were isolated from normalized volumes of supernatants from WT-NPCs, FiNPCs, and AiNPCs after cultured for 12 h, respectively. Purified EVs from three types of NPCs were observed under TEM using negative staining. The figure below shows a partial enlargement of the EVs. (For interpretation of the references to colour in this figure legend, the reader is referred to the web version of this article.)

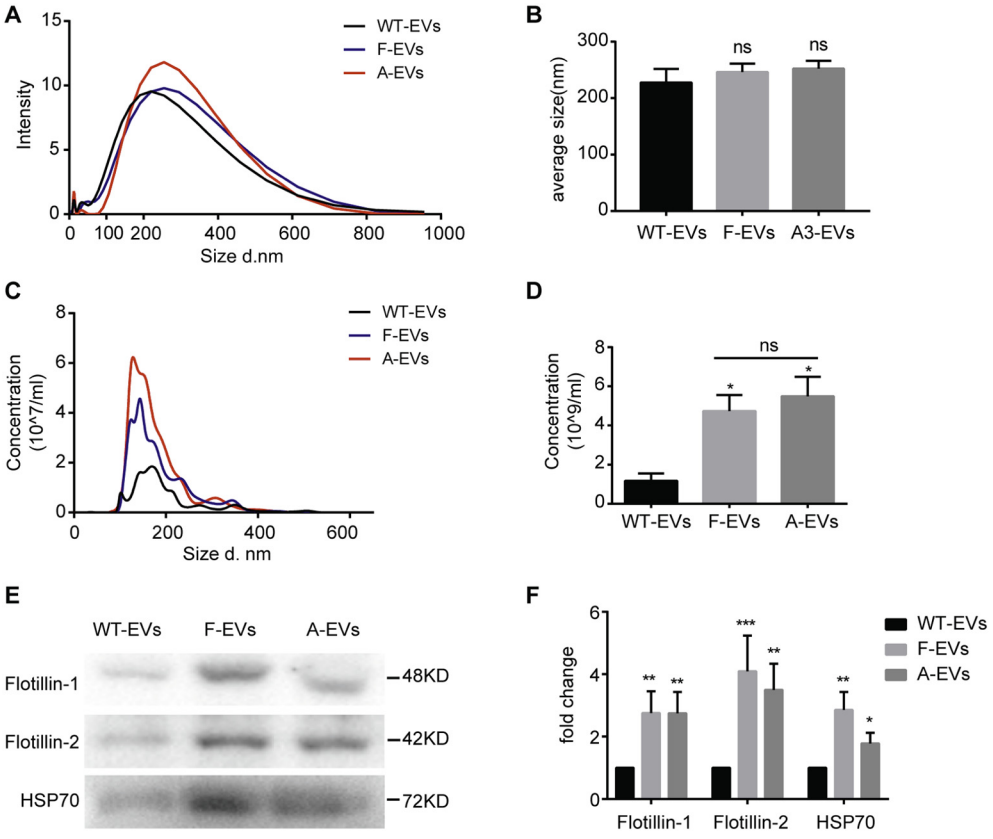

Fig. 2. FiNPCs and AiNPCs secret more EVs than WT-NPCs. (A, B) Particle-size distribution of EVs was determined by Dynamic Light Scattering (DLS). (C, D) Particle-size distribution (C) and concentration (D) of EVs were determined NanoSight analysis (NTA) technologies. (E) Protein lysates were prepared from EV pellets in WT-NPCs, FiNPCs, and AiNPCs. The levels of EVs markers Flotillin-1, Flotillin-2, and HSP70 in EVs were determined by Western blots. (F) Densitometric quantifications of Flotillin-1, Flotillin-2, and HSP70 protein levels were presented as fold change relative to the WT-EVs. Data were represented as mean ± SD from three independent experiments. Statistical differences were measured with one-way ANOVA and *t*-test comparing to WT-EVs. *, **, and *** denote $p < .05$, $p < .01$, and $p < .001$, respectively. ns denotes no significance. Scale bar 500 nm (B).

secretion might be a possible mechanism for the higher proliferative capacities of iNPCs. To test our premise, we investigated the impacts of the three types of EVs on the proliferation of WT-NPCs. 15 μg/ml of EVs were added to WT-NPCs for 24 h, and these EVs were then washed off before the cultures were supplied with the NPC proliferation medium for another 24 h. The NPC proliferation was determined through EdU incorporation assay, which showed a significantly higher proportion of EdU^+ cells in the F-EVs and A-EVs treated groups, compared to the WT-EVs treated controls (Fig. 3A, B). These observations were corroborated by MTS and CCK-8 assays, in which WT-NPCs were first incubated with 15 μg/ml of EVs for 24 h and then cultured with EVs-free conditions for another 48 h in NPC proliferation medium. Both MTS and CCK-8 assays demonstrated higher NPCs viability after the F-EVs and A-EVs treatment compared to the WT-EVs treated controls (Fig. 3C, D). To determine whether the increase of proliferation of WT-NPCs by EVs was dose-dependent, WT-NPCs were cultured with different concentrations (0, 2.5, 5, 10, 15, 20 μg/ml) of EVs (Fig. 3E). Both F-EVs and A-EVs began to promote the proliferation of WT-NPCs at 10 μg/ml concentration. In contrast, WT-EVs had no effect in promoting proliferation at any EVs concentration. We also examined whether the effects of EVs on the proliferation of WT-NPCs was time-dependent. We cultured WT-NPCs with EVs and determined the proliferation of WT-NPCs at several time points (6, 12, 24, 48, 72 h) following EV treatment (Fig. 3F). The proliferation of WT-NPCs significantly increased after treatment with F-EVs and A-EVs for 48 h, compared with those treated with WT-EVs controls. To exclude the effects of EGF and FGF2 in the NPC proliferation medium, we treated WT-NPCs with EVs in growth factor-free NPC basal medium (NeuroCult® NSC Basal Medium) (Fig. S4). Treatment of WT-NPCs with either F-EVs or A-EVs significantly increased the proportions of EdU positive cells, compared with those treated with PBS controls or WT-EVs, indicating a positive effect of F-EVs and A-EVs on NPC proliferation in the absence of EGF and FGF2 growth factors. Therefore, our results suggested that F-EVs and A-EVs induce significantly higher levels of proliferation than those by WT-EVs controls.

3.3. The proteomics analysis of F-EVs, A-EVs and WT-EVs

To identify the molecular contents that may be responsible for the biological activity and regenerative capacity of EVs, we next performed proteomic profiling on these three types of cells and the EVs they secreted. The proteomics analysis revealed that EVs inherit most of the proteins from their parent cells (Fig.4A). Moreover, the expression of growth factor-related domains, such as growth factor receptor cysteine-rich domain, EGF-like domain, and EGF-like calcium-binding domain in EVs, were significantly higher than that in the cells, suggesting growth factor-related proteins are selectively packaged into EVs (Fig. 4B). Interestingly, levels of growth factor-related domains were significantly higher in F-EVs and A-EVs, compared to that in WT-EVs, implying those domains might be the putative factors for the EVs-mediated induction of the WT-NPCs' proliferation (Fig. 4C). The protein domain enrichment analysis was confirmed with KEGG analysis. As expected, KEGG analysis identified multiple growth factor-related signaling pathways that were specifically activated in F-EVs and A-EVs, such as focal adhesion, ECM-receptor interaction and PI3K-AKT signaling pathways (Chaudhary and Hruska, 2001; Kim et al., 2011; Su and Besner, 2014) (Fig. 4D).

3.4. F-EVs/A-EVs activate MEK/ERK pathway

Based on our proteomics analysis, we hypothesized that the growth factor enriched F-EVs and A-EVs might accelerate the proliferation of WT-NPCs through the activation of the downstream pathways of growth factors, MEK/ERK, and PI3K/Akt/mTOR pathway. To test our premise, we first examined whether MEK/ERK pathway and PI3K/Akt/mTOR pathway were activated in WT-NPCs after F-EVs and A-EVs treatment. Due to the presence of EGF and FGF2 in the NPC proliferation medium, which could activate growth factor-related signaling pathways, we treated WT-NPCs with EVs in growth factor-free NPC basal medium (Fig. S5). Since NPC basal medium induces severe cell

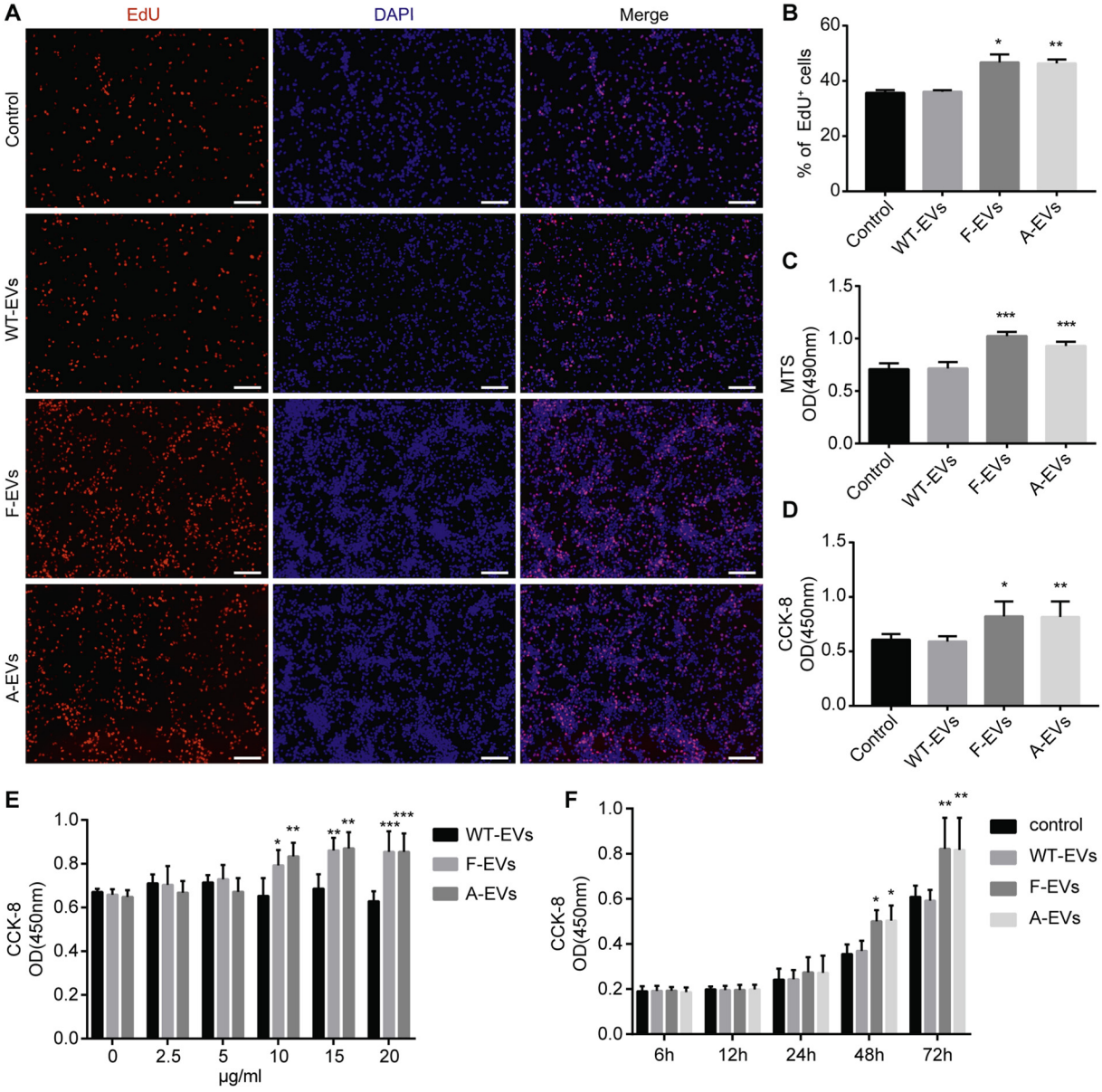

Fig. 3. iNPC-derived EVs facilitate the proliferation of WT-NPCs. (A) WT-NPCs were treated with 15 μg/ml EVs for 24 h, then cultured for 24 h after removal of EVs. EdU was added 2 h prior to fixation. Representative images of EdU (red) and DAPI (blue) staning were shown. (B) Quantification of EdU^+ cells (as a percentage of total cells) in the culture. (C, D) WT-NPCs were treated with 15 μg/ml EVs for 24 h, then cultured for 48 h after removal of EVs. The cell viability of WT-NPCs after EVs treatment was determined by MTS (C) and CCK-8 (D) assays. (E) WT-NPCs were treated with 0, 2.5, 5, 10, 20 μg/ml EVs for 24 h, then cultured for 48 h after removal of EVs. The cell viability of WT-NPCs after the treatment of different concentration of EVs was determined by CCK-8 assay. (F) WT-NPCs were treated with 15 μg/ml EVs for 24 h, then cultured for 48 h after removal of EVs. The cell viability of WT-NPCs at different time windows (6, 12, 24, 48, 72 h) was determined by and CCK-8 assay. Scale bars represent 100 μm (A). Data were represented as mean ± SD from three independent experiments. *, **, and *** denote $p < .05$, $p < .01$, and $p < .001$ in comparison to control, respectively. (For interpretation of the references to colour in this figure legend, the reader is referred to the web version of this article.)

death, we cultured WT-NPCs in NPC basal medium for 1 h (Wang et al., 2016). We found that F-EVs and A-EVs treatment raised the P-MEK (Fig. 5A, C) and P-ERK (Fig. 5A, D) levels significantly, compared to the WT-EVs treated and control groups. However, no significant elevation of the P-Akt levels was observed, suggesting F-EVs/A-EVs might regulate the proliferation capacity of WT-NPCs through MEK/ERK pathway only (Fig. 5A, B). This observation was confirmed by co-culturing EVs with WT-NPCs in NPC proliferation medium for 1 h, in which P-MEK/P-ERK protein levels were higher in F-EVs and A-EVs treated groups, compared to the WT-EVs treated and control group (Fig. S6). Next, we determined the time course of the phosphorylation of MEK and ERK by Western blots. We found that the levels of P-MEK and P-ERK started to show significant increase when WT-NPCs had been treated with F-EVs or A-EVs for 30 min, suggesting a time-dependent activation of the MEK/ERK pathway after F-EVs and A-EVs treatment (Fig. 5E-J). Together, these data indicated that the F-EVs/A-EVs could activate the MEK/ERK pathway, but not the PI3K/Akt/mTOR pathway, in WT-NPCs, while no significant effects of WT-EVs could be observed on both pathways.

3.5. MEK/ERK signaling pathway mediates the F-EVs/A-EVs-induced proliferation of WT-NPCs

To examine whether the F-EVs/A-EVs-induced proliferation of WT-

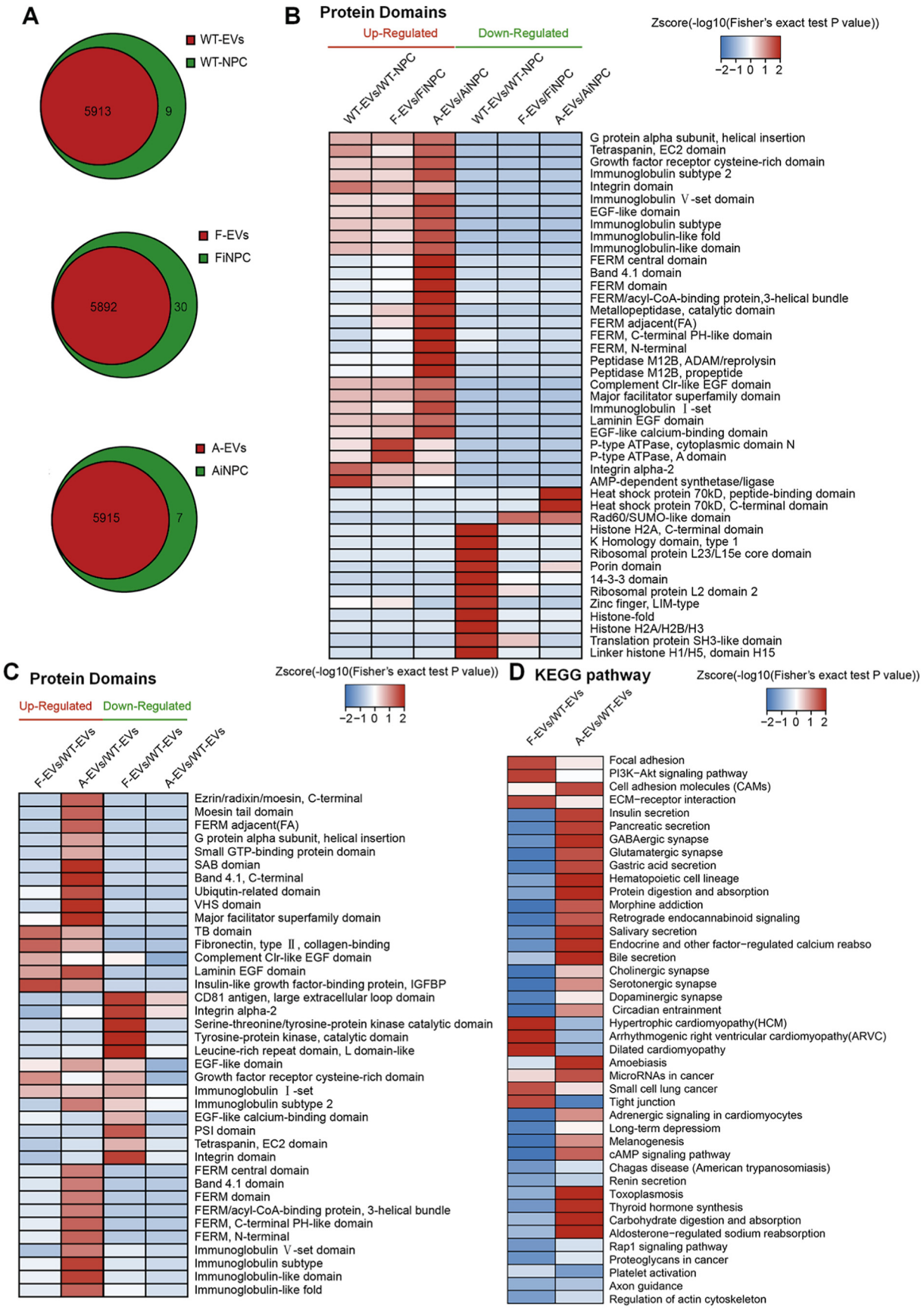

Fig. 4. Proteomics analysis of EVs secreted from WT-NPCs, FiNPCs, AiNPCs. (A) The number of proteins in EVs and NPCs were shown by the Venn diagram. (B) The heat map shown the enrichment of protein domain compared between EVs and their original cells. (C) The heat map shown the enrichment of protein domain compared between F-EVs/A-EVs and WT-EVs. (D) KEGG analysis for the F-EVs and A-EVs enriched protein domains.

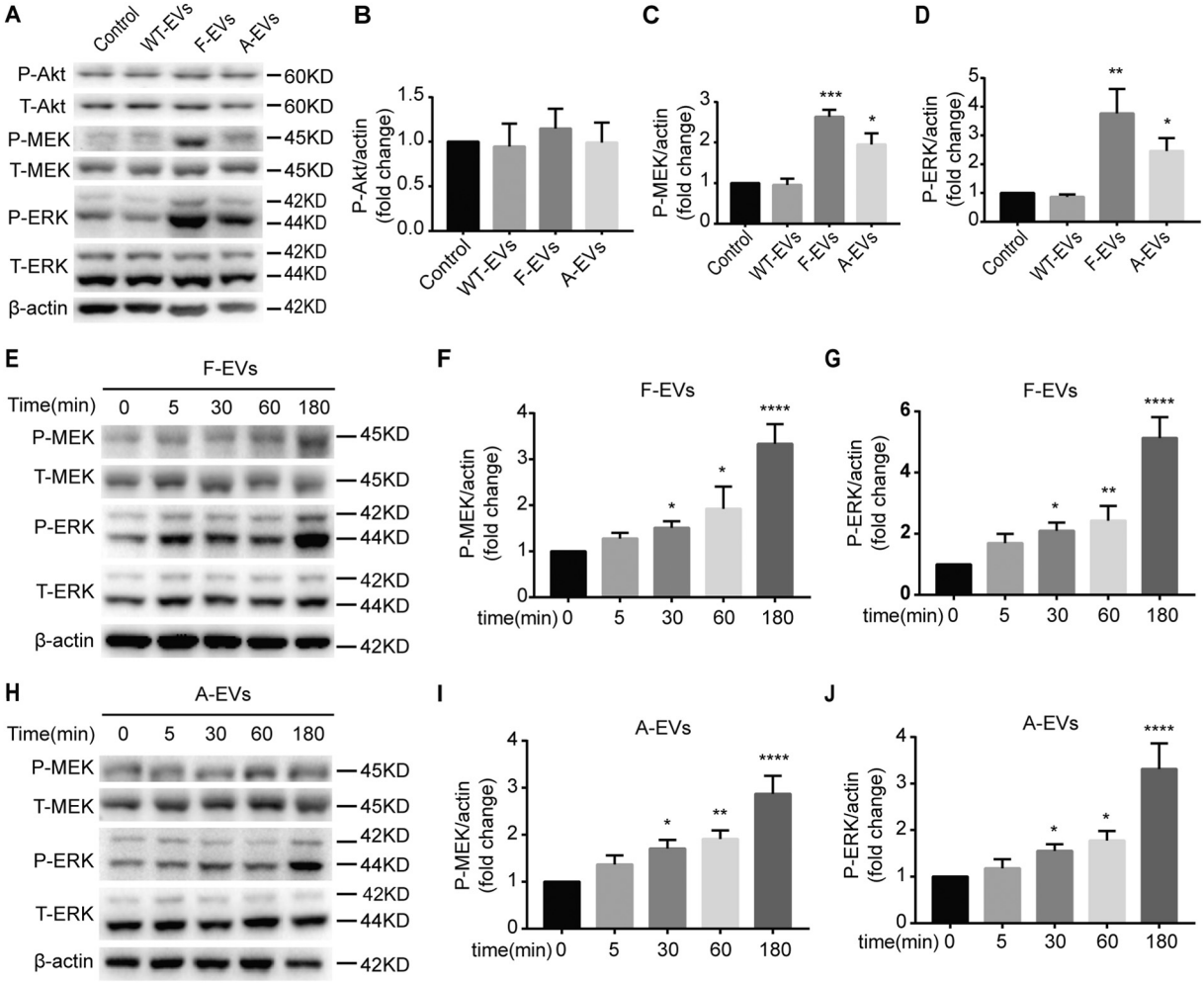

Fig. 5. iNPC-EVs activate the MEK/ERK pathway of WT-NPCs. (A) The representative western blots showing the expression of P-Akt, P-MEK, and P-ERK after three types of EVs treated WT-NPCs for 1 h in NPC basal medium. (B-D) Densitometric quantifications of the P-Akt (B), P-MEK (C) and P-ERK (D) protein levels were presented as fold change relative to the control. (*E*-G) Time course of P-MEK and P-ERK phosphorylation were examined after F-EVs treated WT-NPCs for 0, 15, 30, 60, 180 min in NPC basal medium by Western blot. (H-J) Time course of P-MEK and P-ERK phosphorylation were examined after A-EVs treated WT-NPCs for 0, 15, 30, 60, 180 min in NPC basal medium by Western blot. Data were represented as mean ± SD from three independent experiments. *, **, ***, and **** denote $p < .05$, $p < .01$, $p < .001$, and $p < .0001$ in comparison to control, respectively.

NPCs was mediated by MEK/ERK signaling pathway, we used 10 μM of U0126, which is an ERK1/2 phosphorylation inhibitor (Duncia et al., 1998; Wang et al., 2004), in the treatment of WT-NPCs with different types of EVs in NPC basal medium. The effects of U0126 were validated by Western blots, where the F-EVs- and A-EVs-induced phosphorylation of ERK1/2 in WT-NPCs was blocked (Fig. 6A). The CCK-8 and EdU positive cell quantification further demonstrated that the positive effects of F-EVs and A-EVs on the proliferation of WT-NPCs were blocked by U0126, suggesting that F-EVs and A-EVs might promote the proliferation of WT-NPCs by activating MEK/ERK signaling pathway (Fig. 6B-D).

4. Discussion

Previous studies have shown that transplantation of exogenous neural stem cells could alleviate the symptoms of neurological disorders (Blaya et al., 2015; Lee et al., 2007; Li et al., 2016). However, observations from multiple independent groups have showed that only few exogenous neural stem cells can differentiate into mature neurons and integrate into the neural circuit to replace dead cells after transplantation (Hofstetter et al., 2005; Okada et al., 2005; Skardelly et al., 2011). Therefore, it is likely that exogenous neural stem cells may exert therapeutic effects after transplantation through their capacities in improving the brain microenvironment (Andres et al., 2011; Lu et al., 2003; Minnerup et al., 2011). With the development of reprogramming technology, the therapeutic applications of reprogramming cells have received growing interest within the scientific community (Han et al., 2015; Salewski et al., 2015; Yuan et al., 2013). Although somatic reprogramming provides sufficient sources for NPCs, the effects of those reprogrammed NPCs on the microenvironment are still poorly investigated. Therefore, we reprogrammed mouse fibroblasts and astrocytes into FiNPCs and AiNPCs, respectively, using a defined transcriptional factor set (Sox2, Brn2, Foxg1) (Fig. 7). This is the first time to demonstrate that astrocytes could be reprogrammed into iNPCs, using the same TFs set for fibroblast reprogramming. Due to the same tissue origin and epigenetic memory, AiNPCs may possess more tendencies for neuronal differentiation (Tian et al., 2011). Thus, the reprogramming of various types of patient somatic cells into iNPCs provide promising sources for cell and cell-free therapeutic strategies in treating neurological disorders. Our reprogrammed iNPCs exhibite similar phenotypes of NPCs, except the higher proliferation rate, compared to the WT-NPCs. It might be largely due to the ectopic expression of Sox2 in iNPCs, which was significantly higher than that of WT-NPCs (data not shown). Sox2 functions as a master regulator gene for NPC identity and maintenance (Ellis et al., 2004; Graham et al., 2003), as shown by the fact that knocking down Sox2 expression leads to immediate cell cycle

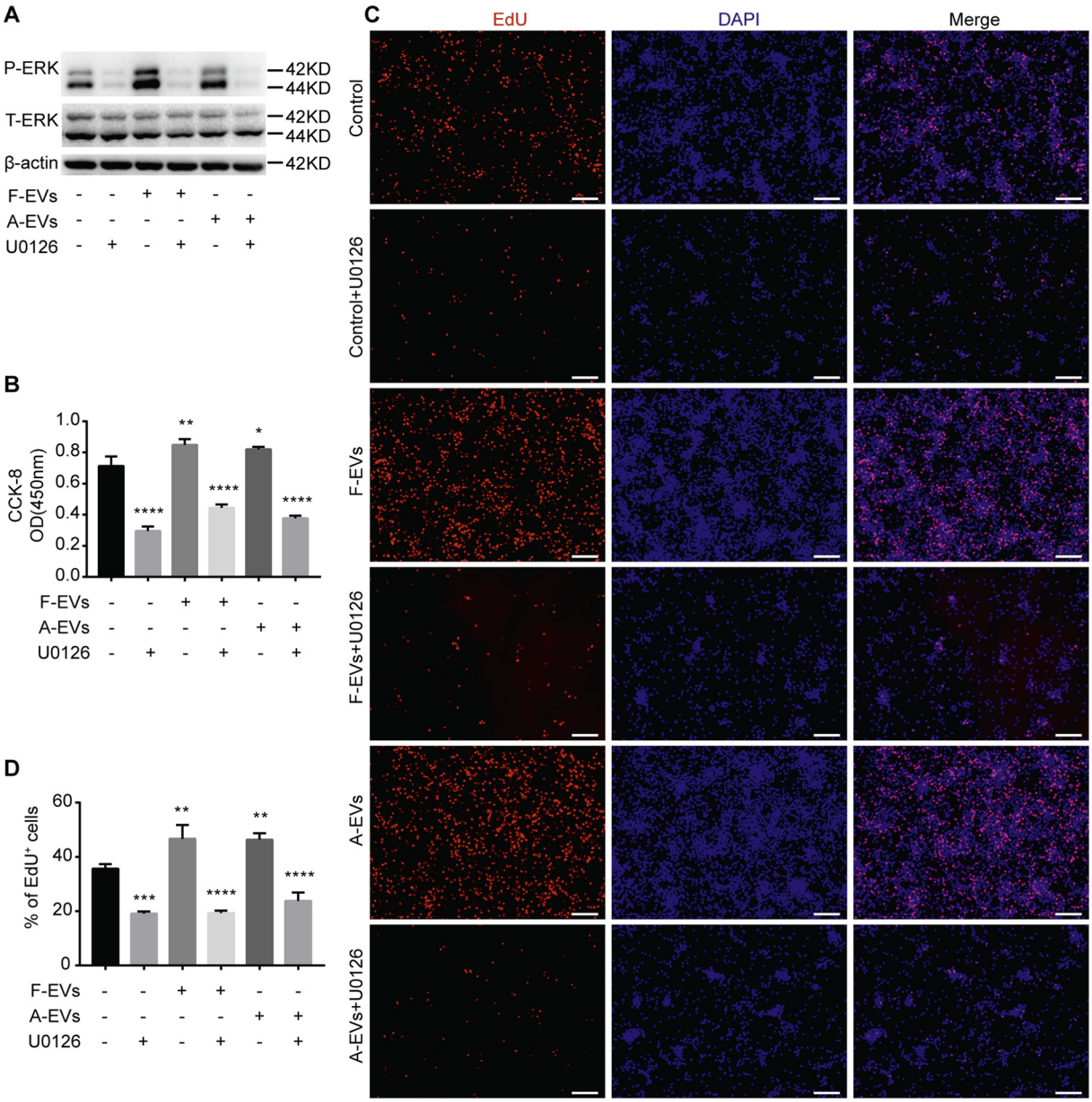

Fig. 6. ERK inhibitor U0126 compromises the positive effects of iNPC-EVs on the proliferation of WT-NPCs. (A) WT-NPCs were cultured with NPC basal medium containing 15 μg/ml F-EVs/A-EVs and 10 μM U0126 for 1 h. The phosphorylation of ERK in different culture conditions was determined by western blot. (B) WT-NPCs were cultured with NPC basal medium containing 15 μg/ml EVs and 10 μM U0126. EVs were removed 24 h after culturing, and the culture was terminated at 48 h after removal of EVs. Cell viability of WT-NPCs was determined by CCK-8 assay. (C) WT-NPCs were cultured with NPC basal medium containing 15 μg/ml EVs and 10 μM U0126. EVs were removed 24 h after culturing, and the culture was terminated at 24 h after removal of EVs. EdU was added 2 h prior to fixation. Representative images of EdU (red) and DAPI (blue) staining were shown. (D) Quantification of EdU^+ cells (as a percentage of total cells) was determined by Image pro plus 6.0. Scale bars represent 100 μm (C). Data were represented as mean ± SD from three independent experiments. ***, **** denote $p < .001$, $p < .0001$ in comparison to control, respectively. (For interpretation of the references to colour in this figure legend, the reader is referred to the web version of this article.)

exit and terminal differentiation of NPCs (Andreu-Agullo et al., 2011; Ferri et al., 2004; Takanaga et al., 2009).

EVs, an important mediator in the communication among cells, are a group of heterogeneous nano-meter-sized membrane vesicles secreted by almost all types of cells, containing enzymes, cytokines, nucleic acids, and bioactive compounds (Colombo et al., 2014). After being released by cells, EVs can alter the local microenvironment, as well as go through the blood-brain barrier and follow the blood and body fluid circulation to other parts of the body to exert its physiological functions (Guay and Regazzi, 2017; Matsumoto et al., 2017; Yanez-Mo et al., 2015). Comparing to iNPCs transplantation, EVs-based therapeutic strategies have unparalleled advantages including high safety without immune response and tumorigenicity (Adamiak et al., 2018; Bobis-Wozowicz et al., 2015; Hu et al., 2015; Wang et al., 2015), simplicity in the collection, storage, and administration. Interestingly, both FiNPCs and AiNPCs produced more EVs than WT-NPCs, suggesting the difference of EV secretion capacity between iNPCs and NPCs is not due to the specific type of reprogrammed cells. Our observation also suggested that iNPCs secreted EVs significantly promoted the proliferation of NPCs. It is highly possible that iNPC-secreted EVs could activate endogenous neural stem cells to proliferate and repair the damaged brain, which will be examined in our future work. In addition, it is also important to explore the effects of iNPC-EVs on other neural cells such as matured neurons and glia.

The proteomics analysis of EVs suggested that the expression levels of growth factor-related proteins such as EGF-like domain, FGF2, IGF1/

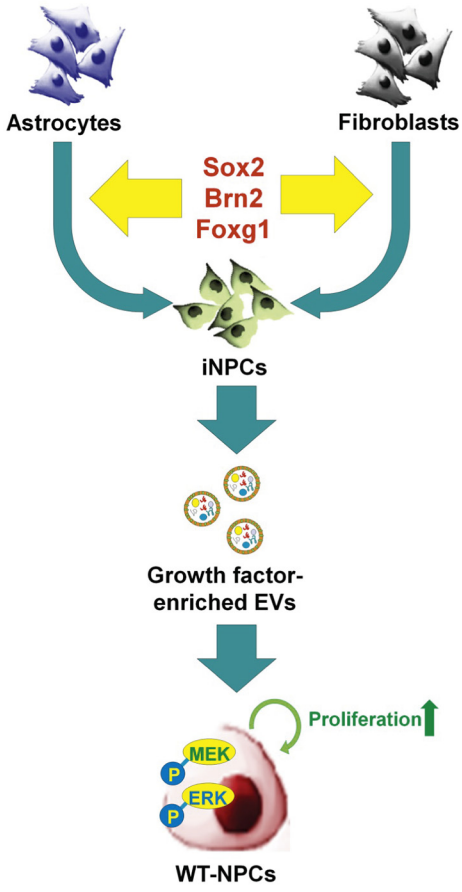

Fig. 7. Proposed model for the involvement of iNPC-derived EVs in the regulation of NPCs' proliferation.
Direct conversion of fibroblasts and astrocytes into iNPCs is achieved by the transduction of same TFs set, Sox2, Brn2, and Foxg1. iNPCs exhibit higher capacity in EVs secretion versus WT-NPCs. Growth factor-related protein domains are preferentially packaged and highly enriched in iNPCs-released EVs. Those EVs accelerate the proliferation of WT-NPCs through activating MEK/ERK pathway.

2r, and IGF2BP2/3 were much higher in iNPC-EVs than in WT-EVs. It has been demonstrated that growth factors are able to enhance the proliferation of NPCs and induce neurogenesis in physiological and pathological conditions (Ohori et al., 2006; Zhao et al., 2007a; Zhao et al., 2007b). Though different growth factors may interact with their specific receptors, they achieve their cellular functions through two down-stream axes, MEK/ERK and PI3K/Akt/mTOR pathways (Fournier et al., 2012; Kalluri et al., 2007; Kim et al., 2006). Many reports have shown that growth factors exert their ability to promote the proliferation of NPCs through the activation of the MEK/ERK pathway. For example, FGF2 and IGF are required to maintain mouse cortical NPCs in a proliferative state through the MEK/ERK pathway (Cheng et al., 2004; Supeno et al., 2013). Moreover, growth factor-enhanced proliferative capacity of NPCs could be suppressed by MEK/ERK pathway inhibitor (Xiao et al., 2007). Our observations revealed that the co-culture of WT-NPCs with iNPC-EVs activated the MEK/ERK pathway and increased the proliferation rate of the former, which could be blocked by a pERK inhibitor. Herein, our data are consistent with the observations reported by other groups.

Another essential down-stream axis of growth factor-related pathways is the PI3K/Akt/mTOR pathway, which is also involved in the regulation of NPC functions (Sato et al., 2010). For example, Zhao et al. have reported that transplanted NPCs could promote the neuroregeneration after brain damage through activation of the PI3K/Akt pathway (Suzuki et al., 2014). However, we did not observe the elevation of phosphorylated PI3K/Akt after EVs treatment, suggesting the inactive status of PI3K/Akt pathway. In cancer cells, multiple reports revealed that there might be a balance of MEK/ERK and PI3K/Akt/mTOR pathways in regulating proliferation and other biological processes (Dai et al., 2009; Hernandez et al., 2013; Jang et al., 2011). It is possible that the combination of growth factors, together with other contents of iNPC-EVs, shift the balance towards the MEK/ERK pathway, which need to be further identified.

In summary, our study identified EVs as a key component of iNPCs-mediated modification of microenvironment, providing a possible mechanism for the therapeutic effect of iNPC transplantation. The proteomics analysis and perturbation of function assay further suggested that the growth factor-enriched EVs regulate NPCs proliferation through the MEK/ERK pathway. We are the first to demonstrate that iNPCs may exhibit distinct influence in modifying the microenvironment in favor of the proliferation of NPCs, compared to WT-NPCs, through secretion of growth factors enriched EVs. Thus, iNPCs-EVs may serve as a promising source in the restoration of the neuronal loss in neurological disorders through expending the endogenous NPCs population and activating neurogenesis in vivo, which are currently being investigated.

Acknowledgments

This work was supported in part by research grants from the National Basic Research Program of China (973 Program Grant No. 2014CB965001 to JZ), Innovative Research Groups of the National Natural Science Foundation of China (#81221001 to JZ), and Joint Research Fund for Overseas Chinese, Hong Kong and Macao Young Scientists of the National Natural Science Foundation of China (#81329002 to JZ), the National Institutes of Health: 1R01NS097195-01 (JZ). We thank Dr. Chao Lin (Tongji University, Shanghai, China) for the assistance with the DLS. We thank Dr. Bin Li (Shanghai Institute of Applied Physics, Chinese Academy of Science) for providing Nanosight NS300. We thank Lenal Bottoms and Justin Peer for proofreading the manuscript.

Author contributions

JCZ YH XX YM KW designed the experiments. YM KW CT YH KM JP ZF performed the experiments. YM KW XX analyzed the data. YM XX YH JCZ prepared the manuscript. All authors read and approved the final manuscript.

Competing financial interests

The authors declare no competing financial interests.

Appendix A. Supplementary data

Supplementary data to this article can be found online at https://doi.org/10.1016/j.nbd.2018.12.003.

References

Adamiak, M., Cheng, G., Bobis-Wozowicz, S., Zhao, L., Kedracka-Krok, S., Samanta, A., Karnas, E., Xuan, Y.T., Skupien-Rabian, B., Chen, X., et al., 2018. Induced pluripotent stem cell (ipsc)-derived extracellular vesicles are safer and more effective for cardiac repair than iPSCs. Circ. Res. 122, 296–309.
Ager, R.R., Davis, J.L., Agazaryan, A., Benavente, F., Poon, W.W., Laferla, F.M., Blurton-Jones, M., 2015. Human neural stem cells improve cognition and promote synaptic growth in two complementary transgenic models of Alzheimer's disease and neuronal loss. Hippocampus 25, 813–826.
Andres, R.H., Horie, N., Slikker, W., Keren-Gill, H., Zhan, K., Sun, G., Manley, N.C., Pereira, M.P., Sheikh, L.A., McMillan, E.L., et al., 2011. Human neural stem cells enhance structural plasticity and axonal transport in the ischaemic brain. Brain 134, 1777–1789.

Andreu-Agullo, C., Maurin, T., Thompson, C.B., Lai, E.C., 2011. Ars2 maintains neural stem-cell identity through direct transcriptional activation of Sox2. Nature 481, 195–198.
Batiz, L.F., Castro, M.A., Burgos, P.V., Velasquez, Z.D., Munoz, R.I., Lafourcade, C.A., Troncoso-Escudero, P., Wyneken, U., 2015. Exosomes as Novel Regulators of Adult Neurogenic Niches. Front Cell Neurosci 9, 501.
Blaya, M.O., Tsoulfas, P., Bramlett, H.M., Dietrich, W.D., 2015. Neural progenitor cell transplantation promotes neuroprotection, enhances hippocampal neurogenesis, and improves cognitive outcomes after traumatic brain injury. Exp. Neurol. 264, 67–81.
Bobis-Wozowicz, S., Kmiotek, K., Sekula, M., Kedracka-Krok, S., Kamycka, E., Adamiak, M., Jankowska, U., Madetko-Talowska, A., Sarna, M., Bik-Multanowski, M., et al., 2015. Human Induced Pluripotent Stem Cell-Derived Microvesicles Transmit RNAs and Proteins to Recipient Mature Heart Cells Modulating Cell Fate and Behavior. Stem Cells 33, 2748–2761.
Chaudhary, L.R., Hruska, K.A., 2001. The cell survival signal Akt is differentially activated by PDGF-BB, EGF, and FGF-2 in osteoblastic cells. J. Cell. Biochem. 81, 304–311.
Chen, Q., Zhang, M., Li, Y., Xu, D., Wang, Y., Song, A., Zhu, B., Huang, Y., Zheng, J.C., 2015. CXCR7 Mediates Neural Progenitor Cells Migration to CXCL12 Independent of CXCR4. Stem Cells 33, 2574–2585.
Cheng, A., Tang, H., Cai, J., Zhu, M., Zhang, X., Rao, M., Mattson, M.P., 2004. Gap junctional communication is required to maintain mouse cortical neural progenitor cells in a proliferative state. Dev. Biol. 272, 203–216.
Colombo, M., Raposo, G., Thery, C., 2014. Biogenesis, secretion, and intercellular interactions of exosomes and other extracellular vesicles. Annu. Rev. Cell Dev. Biol. 30, 255–289.
Corti, S., Nizzardo, M., Simone, C., Falcone, M., Donadoni, C., Salani, S., Rizzo, F., Nardini, M., Riboldi, G., Magri, F., et al., 2012. Direct reprogramming of human astrocytes into neural stem cells and neurons. Exp. Cell Res. 318, 1528–1541.
Dai, R., Chen, R., Li, H., 2009. Cross-talk between PI3K/Akt and MEK/ERK pathways mediates endoplasmic reticulum stress-induced cell cycle progression and cell death in human hepatocellular carcinoma cells. Int. J. Oncol. 34, 1749–1757.
Doeppner, T.R., Herz, J., Gorgens, A., Schlechter, J., Ludwig, A.K., Radtke, S., de Miroschedji, K., Horn, P.A., Giebel, B., Hermann, D.M., 2015. Extracellular vesicles improve post-stroke neuroregeneration and prevent postischemic immunosuppression. Stem Cells Transl. Med. 4, 1131–1143.
Duncia, J.V., Santella III, J.B., Higley, C.A., Pitts, W.J., Wityak, J., Frietze, W.E., Rankin, F.W., Sun, J.H., Earl, R.A., Tabaka, A.C., et al., 1998. MEK inhibitors: the chemistry and biological activity of U0126, its analogs, and cyclization products. Bioorg. Med. Chem. Lett. 8, 2839–2844.
Ellis, P., Fagan, B.M., Magness, S.T., Hutton, S., Taranova, O., Hayashi, S., McMahon, A., Rao, M., Pevny, L., 2004. SOX2, a persistent marker for multipotential neural stem cells derived from embryonic stem cells, the embryo or the adult. Dev. Neurosci. 26, 148–165.
Feliciano, D.M., Zhang, S., Nasrallah, C.M., Lisgo, S.N., Bordey, A., 2014. Embryonic cerebrospinal fluid nanovesicles carry evolutionarily conserved molecules and promote neural stem cell amplification. PLoS One 9, e88810.
Ferri, A.L., Cavallaro, M., Braida, D., Di Cristofano, A., Canta, A., Vezzani, A., Ottolenghi, S., Pandolfi, P.P., Sala, M., Debiasi, S., et al., 2004. Sox2 deficiency causes neurodegeneration and impaired neurogenesis in the adult mouse brain. Development 131, 3805–3819.
Fournier, N.M., Lee, B., Banasr, M., Elsayed, M., Duman, R.S., 2012. Vascular endothelial growth factor regulates adult hippocampal cell proliferation through MEK/ERK- and PI3K/Akt-dependent signaling. Neuropharmacology 63, 642–652.
Goldberg, N.R.S., Marsh, S.E., Ochaba, J., Shelley, B.C., Davtyan, H., Thompson, L.M., Steffan, J.S., Svendsen, C.N., Blurton-Jones, M., 2017. Human neural progenitor transplantation rescues behavior and reduces alpha-synuclein in a transgenic model of dementia with lewy bodies. Stem Cells Transl. Med. 6, 1477–1490.
Goldie, B.J., Dun, M.D., Lin, M., Smith, N.D., Verrills, N.M., Dayas, C.V., Cairns, M.J., 2014. Activity-associated miRNA are packaged in Map1b-enriched exosomes released from depolarized neurons. Nucleic Acids Res. 42, 9195–9208.
Graham, V., Khudyakov, J., Ellis, P., Pevny, L., 2003. SOX2 functions to maintain neural progenitor identity. Neuron 39, 749–765.
Guay, C., Regazzi, R., 2017. Exosomes as new players in metabolic organ cross-talk. Diabetes Obes. Metab. 19 (Suppl. 1), 137–146.
Han, F., Wang, W., Chen, B., Chen, C., Li, S., Lu, X., Duan, J., Zhang, Y., Zhang, Y.A., Guo, W., et al., 2015. Human induced pluripotent stem cell-derived neurons improve motor asymmetry in a 6-hydroxydopamine-induced rat model of Parkinson's disease. Cytotherapy 17, 665–679.
Hernandez, V.J., Weng, J., Ly, P., Pompey, S., Dong, H., Mishra, L., Schwarz, M., Anderson, R.G., Michaely, P., 2013. Cavin-3 dictates the balance between ERK and Akt signaling. elife 2, e00905.
Hessvik, N.P., Llorente, A., 2018. Current knowledge on exosome biogenesis and release. Cell. Mol. Life Sci. 75, 193–208.
Hofstetter, C.P., Holmstrom, N.A., Lilja, J.A., Schweinhardt, P., Hao, J., Spenger, C., Wiesenfeld-Hallin, Z., Kurpad, S.N., Frisen, J., Olson, L., 2005. Allodynia limits the usefulness of intraspinal neural stem cell grafts; directed differentiation improves outcome. Nat. Neurosci. 8, 346–353.
Hou, B., Ma, J., Guo, X., Ju, F., Gao, J., Wang, D., Liu, J., Li, X., Zhang, S., Ren, H., 2017. Exogenous neural stem cells transplantation as a potential therapy for photothrombotic ischemia stroke in Kunming mice model. Mol. Neurobiol. 54, 1254–1262.
Hu, G.W., Li, Q., Niu, X., Hu, B., Liu, J., Zhou, S.M., Guo, S.C., Lang, H.L., Zhang, C.Q., Wang, Y., et al., 2015. Exosomes secreted by human-induced pluripotent stem cell-derived mesenchymal stem cells attenuate limb ischemia by promoting angiogenesis in mice. Stem Cell Res Ther 6, 10.
Huang, Y., Li, Y., Zhang, H., Zhao, R., Jing, R., Xu, Y., He, M., Peer, J., Kim, Y.C., Luo, J., et al., 2018. Zika virus propagation and release in human fetal astrocytes can be suppressed by neutral sphingomyelinase-2 inhibitor GW4869. Cell Discov 4, 19.
Iraci, N., Gaude, E., Leonardi, T., Costa, A.S.H., Cossetti, C., Peruzzotti-Jametti, L., Bernstock, J.D., Saini, H.K., Gelati, M., Vescovi, A.L., et al., 2017. Extracellular vesicles are independent metabolic units with asparaginase activity. Nat. Chem. Biol. 13, 951–955.
Jang, E.R., Kim, Y.J., Myung, S.C., Kim, W., Lee, C.S., 2011. Different effect of protein kinase B/Akt and extracellular signal-regulated kinase inhibition on trichostatin A-induced apoptosis in epithelial ovarian carcinoma cell lines. Mol. Cell. Biochem. 353, 1–11.
Kalluri, H.S., Vemuganti, R., Dempsey, R.J., 2007. Mechanism of insulin-like growth factor I-mediated proliferation of adult neural progenitor cells: role of Akt. Eur. J. Neurosci. 25, 1041–1048.
Kim, S.H., Juhnn, Y.S., Kang, S., Park, S.W., Sung, M.W., Bang, Y.J., Song, Y.S., 2006. Human papillomavirus 16 E5 up-regulates the expression of vascular endothelial growth factor through the activation of epidermal growth factor receptor, MEK/ERK1,2 and PI3K/Akt. Cell. Mol. Life Sci. 63, 930–938.
Kim, S.H., Turnbull, J., Guimond, S., 2011. Extracellular matrix and cell signalling: the dynamic cooperation of integrin, proteoglycan and growth factor receptor. J. Endocrinol. 209, 139–151.
Lai, S., Zhang, M., Xu, D., Zhang, Y., Qiu, L., Tian, C., Zheng, J.C., 2015. Direct reprogramming of induced neural progenitors: a new promising strategy for AD treatment. Transl Neurodegener 4, 7.
Lee, H.J., Kim, K.S., Kim, E.J., Choi, H.B., Lee, K.H., Park, I.H., Ko, Y., Jeong, S.W., Kim, S.U., 2007. Brain transplantation of immortalized human neural stem cells promotes functional recovery in mouse intracerebral hemorrhage stroke model. Stem Cells 25, 1204–1212.
Lee, H., Kang, J.E., Lee, J.K., Bae, J.S., Jin, H.K., 2013. Bone-marrow-derived mesenchymal stem cells promote proliferation and neuronal differentiation of Niemann-pick type C mouse neural stem cells by upregulation and secretion of CCL2. Hum. Gene Ther. 24, 655–669.
Li, X., Zhu, H., Sun, X., Zuo, F., Lei, J., Wang, Z., Bao, X., Wang, R., 2016. Human neural stem cell transplantation rescues cognitive defects in app/ps1 model of alzheimer's disease by enhancing neuronal connectivity and metabolic activity. Front. Aging Neurosci. 8, 282.
Lu, P., Jones, L.L., Snyder, E.Y., Tuszynski, M.H., 2003. Neural stem cells constitutively secrete neurotrophic factors and promote extensive host axonal growth after spinal cord injury. Exp. Neurol. 181, 115–129.
Lujan, E., Chanda, S., Ahlenius, H., Sudhof, T.C., Wernig, M., 2012. Direct conversion of mouse fibroblasts to self-renewing, tripotent neural precursor cells. Proc. Natl. Acad. Sci. U. S. A. 109, 2527–2532.
Ma, K., Deng, X., Xia, X., Fan, Z., Qi, X., Wang, Y., Li, Y., Ma, Y., Chen, Q., Peng, H., et al., 2018. Direct conversion of mouse astrocytes into neural progenitor cells and specific lineages of neurons. Transl Neurodegener 7, 29.
Matsumoto, J., Stewart, T., Banks, W.A., Zhang, J., 2017. The transport mechanism of extracellular vesicles at the blood-brain barrier. Curr. Pharm. Des. 23, 6206–6214.
Minnerup, J., Kim, J.B., Schmidt, A., Diederich, K., Bauer, H., Schilling, M., Strecker, J.K., Ringelstein, E.B., Sommer, C., Scholer, H.R., et al., 2011. Effects of neural progenitor cells on sensorimotor recovery and endogenous repair mechanisms after photothrombotic stroke. Stroke 42, 1757–1763.
Ohori, Y., Yamamoto, S., Nagao, M., Sugimori, M., Yamamoto, N., Nakamura, K., Nakafuku, M., 2006. Growth factor treatment and genetic manipulation stimulate neurogenesis and oligodendrogenesis by endogenous neural progenitors in the injured adult spinal cord. J. Neurosci. 26, 11948–11960.
Okada, S., Ishii, K., Yamane, J., Iwanami, A., Ikegami, T., Katoh, H., Iwamoto, Y., Nakamura, M., Miyoshi, H., Okano, H.J., et al., 2005. In vivo imaging of engrafted neural stem cells: its application in evaluating the optimal timing of transplantation for spinal cord injury. FASEB J. 19, 1839–1841.
Otero-Ortega, L., Laso-Garcia, F., Gomez-De Frutos, M.D., Rodriguez-Frutos, B., Pascual-Guerra, J., Fuentes, B., Diez-Tejedor, E., Gutierrez-Fernandez, M., 2017. White Matter Repair after Extracellular Vesicles Administration in an Experimental Animal Model of Subcortical Stroke. Sci. Rep. 7, 44433.
Raposo, G., Stoorvogel, W., 2013. Extracellular vesicles: exosomes, microvesicles, and friends. J. Cell Biol. 200, 373–383.
Salewski, R.P., Mitchell, R.A., Li, L., Shen, C., Milekovskaia, M., Nagy, A., Fehlings, M.G., 2015. Transplantation of induced pluripotent stem cell-derived neural stem cells mediate functional recovery following thoracic spinal cord injury through remyelination of axons. Stem Cells Transl. Med. 4, 743–754.
Sato, A., Sunayama, J., Matsuda, K., Tachibana, K., Sakurada, K., Tomiyama, A., Kayama, T., Kitanaka, C., 2010. Regulation of neural stem/progenitor cell maintenance by PI3K and mTOR. Neurosci. Lett. 470, 115–120.
Schiera, G., Di Liegro, C.M., Di Liegro, I., 2015. Extracellular membrane vesicles as vehicles for brain cell-to-cell interactions in physiological as well as pathological conditions. Biomed. Res. Int. 2015, 152926.
Shahbazi, E., Moradi, S., Nemati, S., Satarian, L., Basiri, M., Gourabi, H., Zare Mehrjardi, N., Gunther, P., Lampert, A., Handler, K., et al., 2016. Conversion of human fibroblasts to stably self-renewing neural stem cells with a single zinc-finger transcription factor. Stem Cell Reports 6, 539–551.
Skardelly, M., Gaber, K., Burdack, S., Scheidt, F., Hilbig, H., Boltze, J., Forschler, A., Schwarz, S., Schwarz, J., Meixensberger, J., et al., 2011. Long-term benefit of human fetal neuronal progenitor cell transplantation in a clinically adapted model after traumatic brain injury. J. Neurotrauma 28, 401–414.
Su, Y., Besner, G.E., 2014. Heparin-binding EGF-like growth factor (HB-EGF) promotes cell migration and adhesion via focal adhesion kinase. J. Surg. Res. 189, 222–231.
Supeno, N.E., Pati, S., Hadi, R.A., Ghani, A.R., Mustafa, Z., Abdullah, J.M., Idris, F.M., Han, X., Jaafar, H., 2013. IGF-1 acts as controlling switch for long-term proliferation

and maintenance of EGF/FGF-responsive striatal neural stem cells. Int. J. Med. Sci. 10, 522–531.
Suzuki, M., Komuro, K., Ohara, K., 2014. Olanzapine and betamethasone are effective for the treatment of nausea and vomiting due to metastatic Brain tumors of rectal cancer. Case Rep Gastroenterol 8, 13–17.
Takanaga, H., Tsuchida-Straeten, N., Nishide, K., Watanabe, A., Aburatani, H., Kondo, T., 2009. Gli2 is a novel regulator of sox2 expression in telencephalic neuroepithelial cells. Stem Cells 27, 165–174.
Tang, Y., Wang, J., Lin, X., Wang, L., Shao, B., Jin, K., Wang, Y., Yang, G.Y., 2014. Neural stem cell protects aged rat brain from ischemia-reperfusion injury through neurogenesis and angiogenesis. J. Cereb. Blood Flow Metab. 34, 1138–1147.
Tetta, C., Ghigo, E., Silengo, L., Deregibus, M.C., Camussi, G., 2013. Extracellular vesicles as an emerging mechanism of cell-to-cell communication. Endocrine 44, 11–19.
Tian, C., Wang, Y., Sun, L., Ma, K., Zheng, J.C., 2011. Reprogrammed mouse astrocytes retain a "memory" of tissue origin and possess more tendencies for neuronal differentiation than reprogrammed mouse embryonic fibroblasts. Protein Cell 2, 128–140.
Tian, C., Ambroz, R.J., Sun, L., Wang, Y., Ma, K., Chen, Q., Zhu, B., Zheng, J.C., 2012. Direct conversion of dermal fibroblasts into neural progenitor cells by a novel cocktail of defined factors. Curr. Mol. Med. 12, 126–137.
Tian, C., Li, Y., Huang, Y., Wang, Y., Chen, D., Liu, J., Deng, X., Sun, L., Anderson, K., Qi, X., et al., 2015. Selective generation of dopaminergic precursors from mouse fibroblasts by direct lineage conversion. Sci. Rep. 5, 12622.
Wang, Z.Q., Chen, X.C., Yang, G.Y., Zhou, L.F., 2004. U0126 prevents ERK pathway phosphorylation and interleukin-1beta mRNA production after cerebral ischemia. Chin. Med. Sci. J. 19, 270–275.
Wang, Y., Huang, Y., Zhao, L., Li, Y., Zheng, J., 2014. Glutaminase 1 is essential for the differentiation, proliferation, and survival of human neural progenitor cells. Stem Cells Dev. 23, 2782–2790.
Wang, Y., Zhang, L., Li, Y., Chen, L., Wang, X., Guo, W., Zhang, X., Qin, G., He, S.H., Zimmerman, A., et al., 2015. Exosomes/microvesicles from induced pluripotent stem cells deliver cardioprotective miRNAs and prevent cardiomyocyte apoptosis in the ischemic myocardium. Int. J. Cardiol. 192, 61–69.
Wang, Y., Xu, P., Qiu, L., Zhang, M., Huang, Y., Zheng, J.C., 2016. CXCR7 Participates in CXCL12-mediated Cell Cycle and Proliferation Regulation in Mouse Neural Progenitor Cells. Curr. Mol. Med. 16, 738–746.
Wang, K., Ye, L., Lu, H., Chen, H., Zhang, Y., Huang, Y., Zheng, J.C., 2017. TNF-alpha promotes extracellular vesicle release in mouse astrocytes through glutaminase. J. Neuroinflammation 14, 87.
Webb, R.L., Kaiser, E.E., Scoville, S.L., Thompson, T.A., Fatima, S., Pandya, C., Sriram, K., Swetenburg, R.L., Vaibhav, K., Arbab, A.S., et al., 2018. Human neural stem cell extracellular vesicles improve tissue and functional recovery in the murine thromboembolic stroke model. Transl. Stroke Res. 9, 530–539.
Wu, B., Huang, Y., Braun, A.L., Tong, Z., Zhao, R., Li, Y., Liu, F., Zheng, J.C., 2015. Glutaminase-containing microvesicles from HIV-1-infected macrophages and immune-activated microglia induce neurotoxicity. Mol. Neurodegener. 10, 61.
Wu, B., Liu, J., Zhao, R., Li, Y., Peer, J., Braun, A.L., Zhao, L., Wang, Y., Tong, Z., Huang, Y., et al., 2018. Glutaminase 1 regulates the release of extracellular vesicles during neuroinflammation through key metabolic intermediate alpha-ketoglutarate. J. Neuroinflammation 15, 79.
Xiao, Z., Kong, Y., Yang, S., Li, M., Wen, J., Li, L., 2007. Upregulation of Flk-1 by bFGF via the ERK pathway is essential for VEGF-mediated promotion of neural stem cell proliferation. Cell Res. 17, 73–79.
Yanez-Mo, M., Siljander, P.R., Andreu, Z., Zavec, A.B., Borras, F.E., Buzas, E.I., Buzas, K., Casal, E., Cappello, F., Carvalho, J., et al., 2015. Biological properties of extracellular vesicles and their physiological functions. J Extracell Vesicles 4, 27066.
Yarygin, K.N., Kholodenko, I.V., Konieva, A.A., Burunova, V.V., Tairova, R.T., Gubsky, L.V., Cheglakov, I.B., Pirogov, Y.A., Yarygin, V.N., Skvortsova, V.I., 2009. Mechanisms of positive effects of transplantation of human placental mesenchymal stem cells on recovery of rats after experimental ischemic stroke. Bull. Exp. Biol. Med. 148, 862–868.
Yoshimura, A., Adachi, N., Matsuno, H., Kawamata, M., Yoshioka, Y., Kikuchi, H., Odaka, H., Numakawa, T., Kunugi, H., Ochiya, T., et al., 2018. The Sox2 promoter-driven CD63-GFP transgenic rat model allows tracking of neural stem cell-derived extracellular vesicles. Dis. Model. Mech. 11.
Yuan, T., Liao, W., Feng, N.H., Lou, Y.L., Niu, X., Zhang, A.J., Wang, Y., Deng, Z.F., 2013. Human induced pluripotent stem cell-derived neural stem cells survive, migrate, differentiate, and improve neurologic function in a rat model of middle cerebral artery occlusion. Stem Cell Res Ther 4, 73.
Zappulli, V., Friis, K.P., Fitzpatrick, Z., Maguire, C.A., Breakefield, X.O., 2016. Extracellular vesicles and intercellular communication within the nervous system. J. Clin. Invest. 126, 1198–1207.
Zhang, W., Wang, P.J., Sha, H.Y., Ni, J., Li, M.H., Gu, G.J., 2014. Neural stem cell transplants improve cognitive function without altering amyloid pathology in an APP/PS1 double transgenic model of Alzheimer's disease. Mol. Neurobiol. 50, 423–437.
Zhao, L.R., Singhal, S., Duan, W.M., Mehta, J., Kessler, J.A., 2007a. Brain repair by hematopoietic growth factors in a rat model of stroke. Stroke 38, 2584–2591.
Zhao, M., Li, D., Shimazu, K., Zhou, Y.X., Lu, B., Deng, C.X., 2007b. Fibroblast growth factor receptor-1 is required for long-term potentiation, memory consolidation, and neurogenesis. Biol. Psychiatry 62, 381–390.